INFORMATION TO USERS

This manuscript has been reproduced from the microfilm master. UMI films the text directly from the original or copy submitted. Thus, some thesis and dissertation copies are in typewriter face, while others may be from any type of computer printer.

The quality of this reproduction is dependent upon the quality of the copy submitted. Broken or indistinct print, colored or poor quality illustrations and photographs, print bleedthrough, substandard margins, and improper alignment can adversely affect reproduction.

In the unlikely event that the author did not send UMI a complete manuscript and there are missing pages, these will be noted. Also, if unauthorized copyright material had to be removed, a note will indicate the deletion.

Oversize materials (e.g., maps, drawings, charts) are reproduced by sectioning the original, beginning at the upper left-hand corner and continuing from left to right in equal sections with small overlaps.

Photographs included in the original manuscript have been reproduced xerographically in this copy. Higher quality 6" x 9" black and white photographic prints are available for any photographs or illustrations appearing in this copy for an additional charge. Contact UMI directly to order.

UMI®

RICE UNIVERSITY

Inelastic Ion Scattering from Semiconductor Surfaces
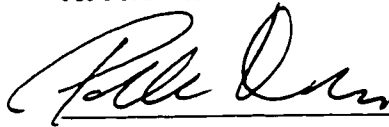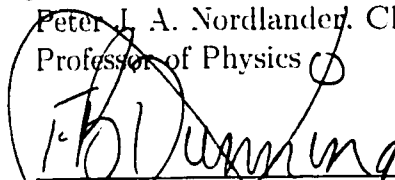
by

John A. Wolfgang

A THESIS SUBMITTED
IN PARTIAL FULFILLMENT OF THE
REQUIREMENTS FOR THE DEGREE

Master of Science

APPROVED, THESIS COMMITTEE:

Peter J. A. Nordlander, Chairman
Professor of Physics

F. Barry Dunning
Professor of Physics

Naomi J. Halas
Professor of Electrical and Computational
Engineering and Chemistry

Houston, Texas

May, 2000

Abstract

Inelastic Ion Scattering from Semiconductor Surfaces

by

John A. Wolfgang

Recent experimental investigations into charge transfer during ion/semiconductor surface collisions indicate dependence of the scattered ion's neutralization probability upon the target surface's local electronic environment along the scattered ion trajectory. This work presents qualitative modeling of these experiments demonstrating how the target surface's local electrostatic potential and charge density modify the scattered ion's neutralization rates. These models have been applied to Ne^+ scattering and S^- recoil from CdS {0001} and {000$\bar{1}$} surfaces as well as Ne^+ scattering from intrinsic, n- and p-doped Si(100)-(2×1) surfaces. Correlation between electrostatic surface potential and ion neutralization probability has been shown for ion scattering from the CdS surfaces. Ne^+ neutralization during scattering from the Si(100)-(2×1) surface correlates to local surface charge density along the ion trajectory. Variations in ion neutralization rate for the intrinsic, n- and p- doped surfaces have been correlated to band bending at the Si surface.

Acknowledgments

Most importantly, I must offer, once again, my unending affection for Miss Bobbie Ross. Throughout the creation of this manuscript she has served as an example of what I have failed to contain within this work, but have managed, by her grace, to capture in life – sublime perfection.

Contents

Illustrations

Tables

Chapter 1

Introduction

Electron charge transfer processes play a fundamental role in many dynamical phenomena at surfaces. The interactions of atoms and molecules with metal surfaces is relatively well understood. Several methods have been developed for the calculation of the energy shift and broadening of atomic and molecular levels near surfaces and for the description of the dynamical interaction between atoms and surfaces in atom-surface scattering experiments. Also a general understanding is beginning to emerge for more complicated charge transfer processes such as Auger neutralization and deexcitation of atoms near metal surfaces. For the case of semiconductors, the situation is far less well understood. While certain features of this interaction have been successfully modeled, no general understanding of the various neutralization and deexcitation channels has emerged.

This work presents an initial qualitative investigation into charge transfer during ion/semiconductor surface scattering events. Several experiments have been successfully modeled, correlating local surface electronic properties to the overall scattered ion neutralization probability. In the first section, scattering of Ne$^+$ ions from CdS {0001} surfaces will be examined. Experimental results indicate that ion neutralization probability is strongly dependent upon the specific scattering trajectory of the

incident ion. This suggests that local variation of the surface electronic structure plays a role in the overall ion neutralization rate. It is shown that the neutralization probability of the scattered ion correlates to local variations in the surface electrostatic potential, as calculated from a density functional approach.

In the second section, Ne^+ ion scattering from an intrinsic, n- and p-doped Si(100)-(2x1) surface will be investigated. As with the scattering of Ne^+ ions from the CdS surfaces, the experimental data for Ne^+ ion scattering from the Si surface suggests that the ion neutralization rate is strongly dependent upon the local electronic structure of the target surface surface along the scattered ion's trajectory. It is shown that a strong correlation exists between local variation of the target surface charge density and the final ion neutralization probability for all three surfaces. However, when comparing the final percentage of neutral ions produced during Ne^+ scattering between n- and p-doped Si target surfaces, significantly fewer neutral ions are produced when scattered from the p-doped surface. This observation can be explained by band bending arguments at the surface, causing dramatic changes in the electrostatic surface potential and influencing the scattered ion neutralization rates.

Chapter 2

Cadmium Sulfide

2.1 Experiment

2.1.1 Experimental Measurement

The experimental investigation of Ne^+ scattering and S^- recoil from a CdS surface was accomplished by Dr. Wayne Rabalais' surface physics group at the University of Houston. Measurement of Ne^+ scattering and S^- recoil from the CdS surface was carried out in a time-of-flight scattering and recoiling spectrometer (TOF-SARS)[1]. The technique uses a pulsed noble gas ion beam which is scattered from a sample surface in an ultra-high vacuum chamber. The scattered and recoiled ions plus fast neutrals are measured by TOF techniques. A 4 keV Ne^+ ion beam with a pulse width of $\sim$50 ns, pulse rate of 30 kHz, and average ion current of $\sim$0.5 nA/cm^2 was used. Ion fraction, Y, measurements were made by using a 50 cm long acceleration tube located within the 90 cm sample to detector drift region. Ions are accelerated by the electric field, thereby separating the ion and neutral fractions in a TOF measurement. The difference in the number of particles measured with no voltage on the deflection plates (neutrals+ions) and with a deflection voltage (only neutrals) gives the absolute number of ions.

CdS has a wurtzite structure which gives rise to a crystallographic polarity, i.e. the surface is terminated in either a Cd or a S layer. Due to the inversion plane, experiments on both the {0001} Cd-terminated and the {000$\bar{1}$} S-terminated surfaces could be made on a single sample by simply rotating the crystal to its opposite side. Both surfaces are unreconstructed and contain two different coexisting domains, rotated by 60° from each other. This results in a 60° structural azimuthal periodicity of the TOF-SARS scans, rather than the 120° periodicity expected for a single domain. For both surface terminations, the primary target atom for the ion beam was Cd. Thus, ion fractions from the Cd-terminated surface reflect collisions from 1st layer Cd atoms, while ion fractions from the S-terminated surface reflect scattering from 2nd-layer Cd atoms.

2.1.2 Ion fraction sensitivity to crystal azimuthal direction δ

Azimuthal scans of the ion fractions were obtained by rotating the crystal about its normal and acquiring TOF spectra at 2° intervals. Both Y_{Ne} and Y_S were found to be highly sensitive to the alignment of the ion beam with the crystal azimuthal directions as well as the nature of the surface termination layer. A periodic behavior as a function of azimuthal angle which is different for the two surface terminations was observed in both Y_{Ne} and Y_S.

The Ne$^+$ ion fractions Y$_{Ne}$ (Fig. 2.1) are higher on the Cd- than the S-terminated surface, and moreover, the maxima and minima have exactly the opposite behavior on these two surfaces when comparison is made under the same angular conditions, i.e., $\alpha = 11^\circ$ and $\beta = 39^\circ$. On the Cd-terminated surface, the lowest values of Y$_{Ne}$ are found along the close-packed atomic rows, i.e., along the azimuths 0° (<1000>), 60° <($0\bar{1}00$)>, and 120° <(0010)>. The Ne$^+$ neutralization probability is hence enhanced, or comparably, the ion survival probability is decreased, along these dense Cd rows. Minima are also observed along the 30° <($1\bar{1}00$)> and 90° <($0\bar{1}10$)> azimuths, however they are not as deep as those along the close-packed directions. The observed periodicity of the oscillations is 30°. On the S-terminated surface (Fig. 2.1), the highest values of Y$_{Ne}$ are found along the principal azimuths, i.e., 0°, 30°, 60°, and 90°, and they exhibit a 30° periodicity. Due to the low incident angle of $\alpha = 11°$, the trajectories of the incident Ne$^+$ ions are influenced by grazing multiple collisions with first-layer S atoms. In order to correctly model the ion scattering, knowledge of the ion scattering trajectories is necessary. The classical ion trajectory simulation program called scattering and recoiling imaging code[2] (SARIC) was used to simulate the trajectories of the incident and exit atoms. SARIC is based on the binary collision approximation, uses screened Coulomb potentials to describe the interactions between atoms, and includes both out-of-plane and multiple scattering.

An analysis of the trajectories using the SARIC program shows that this multiple scattering effect is particularly pronounced along the high symmetry azimuths at 0°, 30°, 60°, etc. This is known as quasi-single scattering, where the projectile makes several small angle deflection collisions with S atoms and a single large angle deflection collision with a Cd atom: the latter collision determines the final scattered ion energy. The structure of the CdS surface, with its short first-layer S to second-layer Cd spacings (0.84 Å), long second-layer Cd to third-layer S spacings (2.51 Å), and short lateral spacings between the first-layer S and second-layer Cd (1.19 Å), emphasizes such multiple scattering collisions. The experiment thus implies high Y_{Ne} along trajectories involving Ne^+ motion close to first-layer S atoms.

2.1.3 S⁻ Recoil

The S⁻ ion fractions Y_S (Fig. 2.2) are higher on the Cd- than on the S-terminated surface, as is Y_{Ne}. On the Cd-terminated surface, Y_S exhibits the exact same periodicity with maxima and minima at the same positions as Y_{Ne} (Fig.2.1). The lowest values of Y_S are found along the close-packed Cd atomic rows. The S⁻ neutralization probability is hence enhanced, or comparably, the ion survival probability is decreased, along these dense Cd rows. The observed periodicity of the oscillations is 30°. Due to the relatively low exit angle of $\beta = 19°$, the trajectories of the recoiled second-layer S atoms are influenced by multiple collisions with first-layer Cd atoms.

An analysis of the trajectories using the SARIC program in a manner similar to that described above shows that this effect is particularly pronounced along the high symmetry azimuths at 0°, 30°, 60°, etc. similar to that observed for Ne^+ scattering from Cd on the S-terminated surface. This result implies that low Y_S is obtained along trajectories involving S^- motion close to first-layer Cd atoms. On the S-terminated surface, Y_S exhibits a 60° periodicity and the highest values of Y_S are found along the 30°, 90°, and 150° directions, where the density of Cd atoms is lowest. These results clearly demonstrate that both Y_{Ne} and Y_S are sensitive to the surface structural corrugation as well as the elemental composition.

2.2 Theoretical Approach

2.2.1 Overview

A qualitative model has been created to describe the charge transfer dynamics during Ne^+ scattering and S^- recoil from the CdS surface. A description of the electronic structure of the CdS target surface was calculated using a quantum chemical approach, implementing a density functional algorithm. This model was used to determine the electrostatic potential above the Cd target surfaces. From this surface model a simple rate equation approach for charge transfer between the scattered ion and the CdS surface was applied to describe the final ion fraction observed in the experimental data.

2.2.2 Electronic Structure of Small CdS Clusters

The electronic structure of a wurtzite CdS surface was calculated using a density functional algorithm utilizing the von Barth and Hedin [3] local spin density (LSD) approximation for exchange/correlation effects. Our scalable parallel code allows for *ab initio* calculation of electronic structure as well as geometry optimization and has been successfully tested for a variety of parallel architectures[4]. The use of numerical basis sets allows this algorithm to provide a very accurate description of the electronic structure of clusters with fast cpu times[5].

A finite cluster was used to model the physical semiconductor surface. Calculations were made for four different CdS clusters of varying size (Fig. 2.3), from 14 to 74 atoms with up to eight layers (Cd-S-Cd-S-Cd-S-Cd-S). Geometric information for these model systems was taken from previous experimental work[6]. For consistency, the clusters were created with the stoichiometry of the physical system. This allowed for a comparison of the electronic properties of both the Cd- and the S-terminated surfaces on the same cluster. As will be discussed below, the key microscopic feature of the surface influencing the charge transfer is the lateral variation of the charge density and electrostatic potential near the surface[7]. We therefore included tests for uniformity in charge density and local atomic charge state in determining the optimal cluster to be used. Final comparison of known electronic proper-

ties, such as the band gap, help gauge the validity of the model to the experimental system.

An analysis of the atomic Mulliken populations for the set of modeled clusters yields a qualitative picture of the charge coordination for individual atomic sites within the cluster. Variation of the Mulliken population measured between the central atom and its nearest neighbor for the four different clusters is presented in table 2.1. The 74 atom, four layer (Cd-S-Cd-S) cluster shows the greatest uniformity, indicating that the lateral dimension is the most relevant structure factor for cluster convergence.

A more rigorous test of cluster convergence involved an analysis of the deformation density along equivalent regions of the surfaces of the different clusters. The deformation density, being the difference between the interacting cluster charge density and the charge density from the neutral atoms, is a sensitive probe of inhomogeneity in the valence charge density distribution caused by finite cluster size effects. The deformation charge density in a region of the cluster surface including the central surface atom and its nearest neighbors was calculated for each cluster and termination. By calculating the root mean square (rms) deviation of these deformation charge densities between different clusters it is possible to check the cluster convergence. For sufficiently large clusters, we expect this rms deviation to be zero.

The results of this analysis are presented in table 2.2. It can be seen that as the size of the cluster is increased, the variation between successively larger clusters

decreases. The smallest cluster A shows the largest differences between all larger clusters, indicating a poorly converged model system. The differences between the C and D clusters is roughly an order of magnitude smaller than the difference between clusters A and D. Table 2.2 clearly shows that cluster D provides the most uniform surface charge density and is therefore best suited to model the physical surface.

Finally, a comparison of the calculated HOMO/LUMO gap to the experimentally reported band gap provides a test for convergence to a real system. The calculated HOMO/ LUMO gaps were 0.72, 1.46, 1.91, and 2.36 eV for clusters A, B, C, and D, respectively. A reported value of 2.582 eV for CdS [8, 9] provides yet another indication that cluster D best models the properties of a CdS surface. Taking this 74 atom cluster D as our model system, a variety of properties relevant to the discussion of Ne^+ scattering and S^- recoiling from CdS were calculated.

2.2.3 Charge density and electrostatic potential

The Mulliken population charge analysis yields charge states of +0.55 and -0.55 electrons for surface Cd and S atoms, respectively. This indicates that the bonding occurs through charge donation from Cd to S, resulting in a slightly ionic bond. This electronic rearrangement can be observed directly from the deformation density plots of the cluster surfaces and cross sections, Fig. 2.4. A strong local increase in charge density near the S atom is observed for both surface and bulk sites. A corresponding

depletion of charge around the Cd atoms is clearly observed. This charge rearrangement appears as a somewhat spherical uniform charge variation, again reflecting ionic rather than covalent bonding. The Mulliken charge state increases for atoms in the interior of the crystal, reflecting the slight increase in Madelung potential for bulk sites compared to surface sites. The nonuniform charge distribution at the surface atoms results in a lateral modulation of the electrostatic potential. Due to the positive charge near Cd atoms, the electrostatic potential is slightly positive in the vicinity of Cd atoms. Near S atoms, the situation is opposite. Due to the accumulation of electrons near the S atoms, the electrostatic potential is negative in their vicinity.

2.2.4 Density of states

Calculation of the density of states (DOS) and projected density of states (PDOS) provides a detailed description of the electronic structure of the CdS surfaces. The total density of states (Fig. 2.5) for CdS indicates a band gap of 2.36 eV, compared to literature values of 2.582 eV at 0 K and 2.42 eV at 300 K[8, 9]. An analysis of the PDOS for Cd and S indicates that the valence states of the CdS system are composed mostly of the $S(3p)$ and $Cd(5s)$ states of the surface atoms. The strongest contribution to the occupied DOS comes from the $S(3p)$ state, whereas the contribution by the $Cd(5s)$ state is negligible. The predominant weight of the $Cd(5s)$ orbital appears in the unoccupied DOS, reflective of the charge transfer from Cd to S. The degree of

ionicity is larger for atoms in bulk-like sites than for surface sites. This is caused by the difference in the Madelung potential between surface and bulk sites. Such a change in potential creates a shift of orbital energies, resulting in Tamm surface states[10]. These states "crowd" the band gap, reducing its size compared to the bulk condition. This effect is clearly observed in our calculated PDOS for the S(3p) valence atomic states. The predominant weight of the PDOS for the S(3p) state is located at higher energy for the surface sites compared to the PDOS for the second-layer S sites. This shift and resulting introduction of surface states causes a reduction of the band gap and may explain the difference between the calculated band gap and the experimental data.

2.2.5 Modeling the surface

One of the key features determining the electron transfer rates between a surface and an atom is the electrostatic potential between the atom and the surface[7]. In order to understand the charge transfer involved in Ne^+ scattering and S^- recoiling from the CdS surface, it is necessary to have a model of the surface which exhibits the correct periodicity. To model the surface with a finite cluster one must therefore repeat the electrostatic potential of a fully converged surface unit cell with the appropriate lattice basis vectors.

Since the electrostatic potential is relatively long range, one would expect that a relatively large cluster would be needed to converge the potential in a unit cell. In order to check the convergence of the electrostatic potential of our clusters, we examined the difference in the electrostatic potential in a surface unit cell between clusters of increasing size. This difference was found to be essentially zero between clusters C and D.

The electrostatic potential outside the Cd-terminated surface is shown in Fig. 2.6-A. The figure clearly shows a sharp increase in the electrostatic potential in the region above the Cd atoms (visible as white patches in a hexagonal lattice). This is caused by the depletion of electrons near the Cd atoms. The influence of the S atoms in the second-layer is small and can barely be observed. The electrostatic potential outside the S-terminated surface is shown in Fig. 2.6-B. The decreased electrostatic potential above the S atoms in the first-layer is visible as the hexagonal array of dark patches. The figure also shows an increased electrostatic potential above the Cd atoms in the second-layer in the form of a hexagonal array of white patches.

2.2.6 Charge Transfer Dynamics

2.2.7 Neutralization of Ne^+

At a collision energy of 4 keV and scattering angle of $50°$, the corresponding impact parameter for Ne^+ scattering from Cd is 0.790 a.u[11]. The positive ions scattering

on the surface can be neutralized in the close encounter with the Cd atoms or by electron capture along the incoming and outgoing trajectories. Neutralization during the close encounter can be an efficient process[12], however it is not likely to introduce an azimuthal dependence of the ion fractions. Neutralization of the Ne^+ ion can occur through resonant tunneling into the Ne(3s) level and through Auger deexcitation and Auger neutralization[12]. In all three cases, an electron is transferred from the crystal through the surface into the atom. An important factor in determining the neutralization rate is therefore whether a potential energy barrier for the electron exists between the atom and the surface. In previous investigations[7] of electropositive and electronegative impurities chemisorbed on metal surfaces, it was found that the electrostatic barriers introduced by impurity atoms can change the electron tunneling rates by orders of magnitude[7]. The finding of a large spatial variation of the electrostatic potential outside the CdS(0001) surfaces implies that the lateral variation of the electron transfer rates may be substantial. The increased electrostatic potential in the vicinity of the Cd atoms translates into reduced potential energy barriers for electron tunneling between the surface and an atom in the vicinity a surface Cd atom. The decreased electrostatic potential above the surface S atoms is equivalent to a potential energy barrier for an electron tunneling between the surface and an atom above a S site. We therefore expect electron transfer rates to be smaller above S atoms than above Cd atoms in the top layer. The present experimental data on

the neutralization of Ne$^+$ atoms scattered from the Cd- and S-terminated surfaces is indeed consistent with this idea. The experimental results of Fig. 3 are consistent with large neutralization probabilities along trajectories that pass above Cd-rich regions of the surface and low neutralization probabilities above S-rich regions of the surface.

2.2.8 Charge transfer model

The neutralization of the Ne$^+$ atoms scattered from the surface can be modeled by integrating the following simple rate equation[13, 14]

$$dn(t)/dt = \Gamma[\vec{R}(t)]n(t) \tag{2.1}$$

along the ion trajectory $\vec{R}(t)$. It is assumed that the ion trajectories start at a large distance from the surface and that the motion of the ions is straight and with constant velocity. The Ne$^+$ ions are assumed to turn at a distance equivalent to the impact parameter of 0.79 a.u. in a collision with a Cd atom [11]. $\Gamma[\vec{R}(t)]$ is the instantaneous neutralization rate of Ne$^+$ at position $\vec{R}(t)$. Since the surface contains two domains oriented at 60° with respect from each other, the final charge transfer in one direction has to be averaged over both domains. The electron transfer probabilities $\Gamma[\vec{R}(t)]$ are modulated by the potential barriers caused by the inhomogeneous electrostatic

potential near the surface. For simplicity, we assume that the electron transfer rates can be written as

$$\Gamma[\vec{R}(t)] = \Gamma_Z(Z) \times \xi_A(\rho), \tag{2.2}$$

where ρ is the lateral distance between the scattered atom and the nearest substrate atom in the top layer. A reasonable fit to the neutralization rates on both the Cd- and S-terminated surfaces is obtained by assuming the following saturated exponential form for Γ_Z : $\Gamma_Z(Z) = 0.01$ a.u. for ion-surface distances $Z < 3$ a.u. and $\Gamma_Z(Z) = 0.01\exp[-(Z-3)]$ a.u. for $Z > 3$ a.u. For simplicity, we parameterize the lateral modulation of the electron tunneling rates as $\xi_A(\rho) = \xi_A^\circ$ for $\rho < R_A$ and $\xi_A(\rho) = 1$ for $\rho > R_A$.

2.3 Results

2.3.1 Cd-terminated Surface Ne^+ Scattering

A good fit of the experimental data of Fig. 2.1 for Ne^+ scattered from the Cd-terminated surface is obtained by assuming $R_{Cd} = 2.5$ a.u. and $\xi_{Cd}^\circ = 2$. Such an enhancement of the electron tunneling rates above a Cd atom on the surface is consistent with the increased electrostatic potential in the vicinity of the Cd atom. The results of the calculation are shown in Fig. 2.7-A. In this figure we also show the sensitivity of the calculated neutralization probabilities to variations in the radius

R_{Cd}. It can be seen that the results are qualitatively similar, with decreased ion fractions along Cd-rich azimuths.

2.3.2 S-terminated Surface Ne^+ Scattering

On the S-terminated surface the situation is more complicated. Due to the low incident angle of $\alpha = 11°$, the trajectories of the incident Ne^+ ions are influenced by grazing multiple collisions with first-layer S atoms. An analysis of the trajectories using the SARIC program,14 shows that quasi-single scattering is particularly pronounced along the high symmetry azimuths at 0, 30, 60°, etc.

In order to model the relatively complicated multiple Ne-S collisions occurring along the incident trajectory on the S-terminated surface, two different trajectories were used to calculate the charge transfer processes on this surface. In trajectory A, the ion impacts the Cd atom in the second-layer. In trajectory B, the atom is assumed to impact a fictitious Cd atom in the second-layer just below a top layer S atom. The choice of this trajectory was motivated by an analysis of the atomic trajectories in the high symmetry directions. The analysis showed that for incoming trajectories along these directions, almost all of the Ne particles passed within 2.5 a.u. from first-layer S atoms. Trajectory B possesses exactly this property. The final charge transfer on the S-terminated surface is simply taken as the average of the charge transfer along these two trajectories, $n(d) = \alpha_{AB} n_A(\delta) + (1 - \alpha_{AB}) n_B(\delta)$. For

simplicity, the parameter α_{AB} is taken as 1/2. Using the same radius $R_S = 2.5$ a.u. as in Ne scattering from the Cd-terminated surface, a reasonable fit of the experimental data is obtained using $\xi_S^0 = 1/3$. Such a reduction of the electron tunneling rates above a S atom on the surface is consistent with the decreased electrostatic potential in the vicinity of the S atom. The calculated azimuthal variation of the ion fraction is shown in Fig. 2.7. The figure also shows how the final ion fraction depends on our trajectory parameter α_{AB}. It can be seen that the results are qualitatively similar with increased ion fractions along S-rich azimuths.

The calculation shows larger ion fractions for Ne scattering from the Cd-terminated surface than from the S-terminated surface, in agreement with experimental results (Fig. 2.1). The reason for this is simply that on the S-terminated surface, the ions emerge from a second-layer atom so that they travel a larger distance close to the surface and hence have a higher probability of becoming neutralized.

The magnitude of the lateral corrugation of the electron tunneling rates obtained from fitting the experimental data are consistent with the results from the density functional calculations. In a previous study of a hydrogen atom near a potassium atom chemisorbed on a metal surface, it was found that the width of the lowest hydrogen levels could increase by a factor between 2 and 5 right above the potassium atom compared with the width outside of a clean surface. For a hydrogen atom above a chemisorbed chlorine atom, the widths were found to decrease by similar

factors[7, 15]. With Mulliken charges of -0.55 on Cd and +0.55 on S on the CdS surface, it is not surprising to find similar enhancements and reductions above the surface Cd and S atoms.

2.3.3 Recoil of S⁻ Ions

The same theoretical approach can be used to model the formation of S⁻ during recoiling of S from the surface. An analysis using the SARIC program shows that the trajectories of S⁻ recoiled from the Cd-terminated surface become very complicated with multiple small angle collisions. We therefore focus our attention on S⁻ recoil from the S-terminated surface. Since the recoiling is from the first-layer, the trajectories are simple without any collisions. Equation 2.1 is solved for a S atom moving from its site in the top layer to a sufficiently large distance from the surface such that the charge transfer has ceased. It is assumed that the negative ion fraction of recoiled S atoms is zero at the start of the trajectory. The electron capture rates are different for S than for Ne on CdS. The overall charge transfer is best fitted using $\Gamma_Z(Z) = 0.001$ a.u. for ion-surface distances $Z > 2$ a.u. and $\Gamma_Z(Z) = 0.001\exp[-1.2(Z-2)]$ a.u. for $Z > 2$ a.u. As before, Eq. 2.2 is used to describe the lateral modulation of the electron tunneling rates between the S atom and the surface. A reasonable fit of the experimental results of Fig. 2.2 gave $R_S = 3.0$ a.u. and $\xi_S^o = 1/3$. Such a reduction of the electron tunneling rates above a S atom on the surface is consistent with the

increased electrostatic potential in the vicinity of the S atoms. Fig. 2.8 shows the calculated azimuthal variation of the S^- ion fractions from the S-terminated surface. Also shown is the final ion fraction dependence on the parameter ξ_S^0. It can be seen that the results are qualitatively similar, with increased ion fractions along S poor azimuths in the 30° and 90° directions.

Table 2.1 Atomic Mulliken Charge Deviation Between Nearest Neighbors. Charge differences. $\Delta q(n)$, are reported by number of electrons. X/Y. where n indicates the specific layer of cluster($n=1$ being the surface), X is the Cd layer and Y is the sulfur layer charge difference.

Cluster	atoms	layer	$\Delta q(1)$	$\Delta q(2)$	$\Delta q(3)$
A	14	1	0.090/0.084	–	–
B	26	2	0.051/0.057	0.032/0.126	–
C	52	4	0.069/0.207	0.011/0.094	0.002/0.063
D	72	2	0.014/0.002	0.004/0.002	–

Table 2.2 Root Mean Square Deviation of Deformation Density Between CdS Planes. The charge difference between two cluster surface planes is reported by number of electrons. X/Y, where X corresponds to the Cd and Y to the S-terminated rms deviation.

Cluster	B	C	D
A	1.86E-04/7.71E-04	2.02E-04/9.01E-04	4.51E-04/1.07E-03
B	–	2.01E-04/3.95E-04	2.21E-04/4.43E-04
C	–	–	6.35E-05/8.11E-05

22
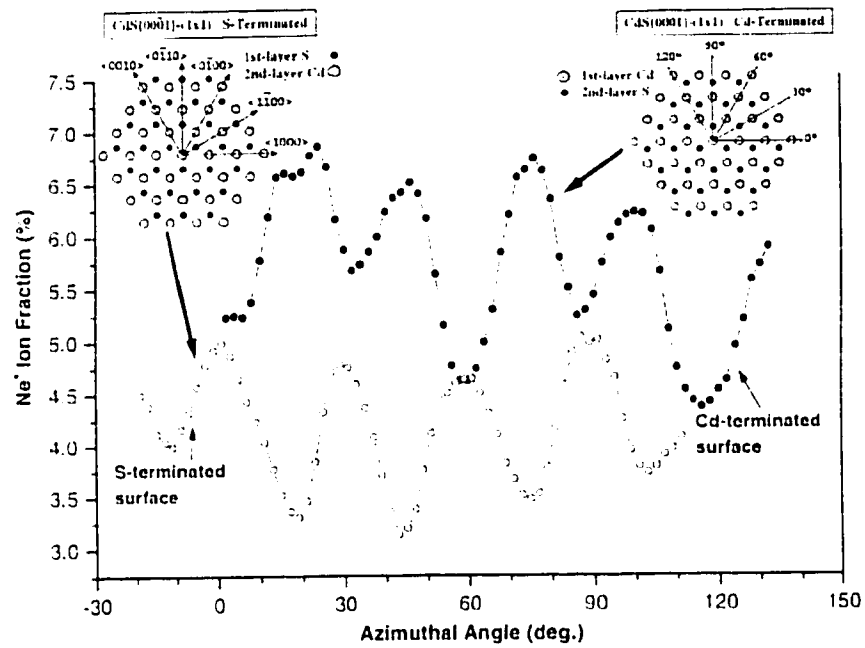
Figure 2.1 Scattered Ne⁺ ion fractions versus azimuthal angle δ for the Cd- and S-terminated surfaces. Solid circles - Cd-terminated surface. Open circles - S-terminated surface. Schematic diagrams of the two surface configurations are included.
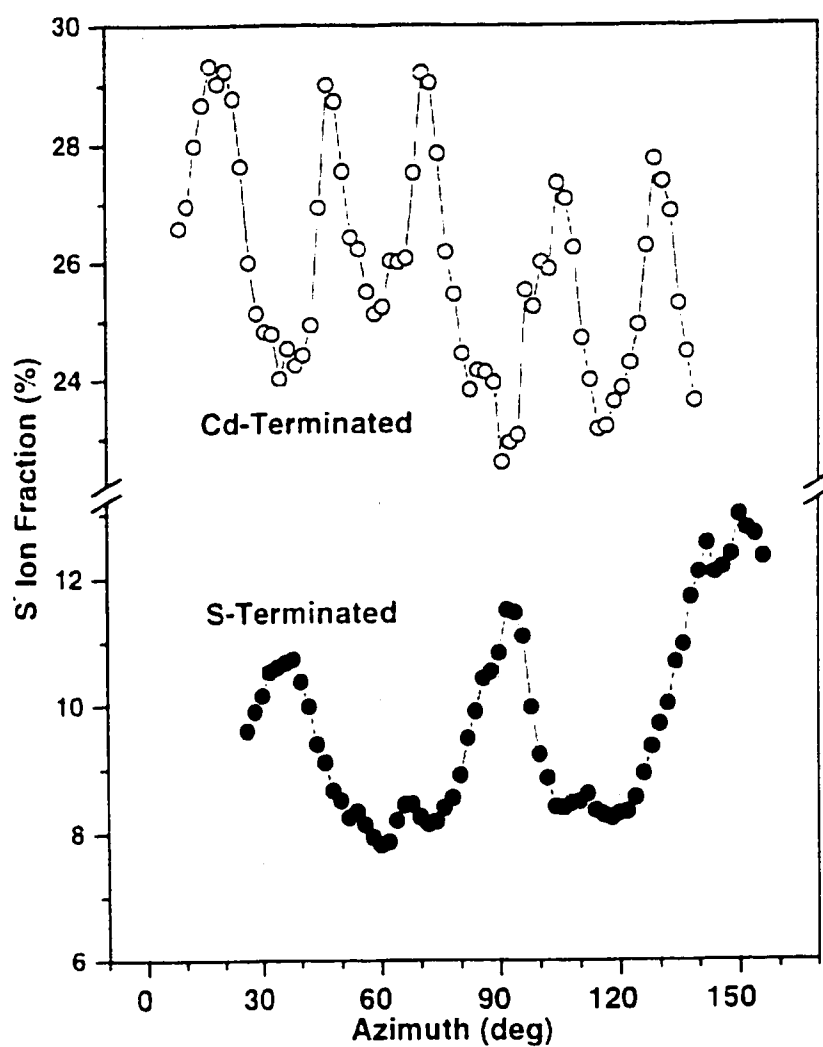
Figure 2.2 Recoiled S⁻ ion fractions versus azimuthal angle, δ, for the Cd- and S-terminated surfaces. Solid circles - S-terminated surface. Open circles - Cd-terminated surface.
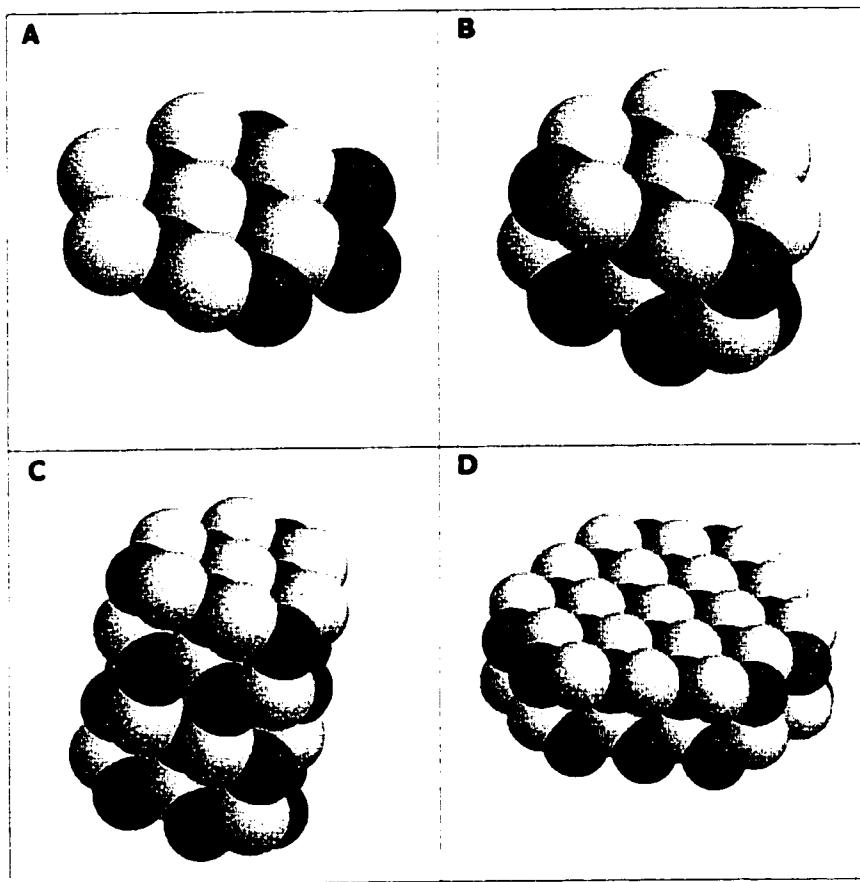
Figure 2.3 Geometrical structure of CdS clusters used to model the electrostatic surface potential. A) 14 atoms, one layer (Cd-S); B) 26 atoms, two layers (Cd-S-Cd-S); C) 52 atoms, four layers; D) 72 atoms, two layers.
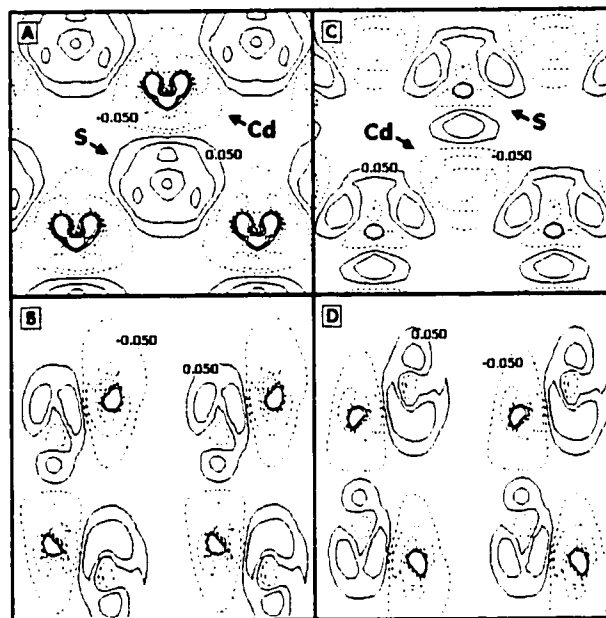
Figure 2.4 Electron Deformation density plots for CdS cluster D of Fig. 2.3. Figures A and B represent surface and cross-sectional cuts (along δ = 90° azimuth), respectively for a Cd-terminated surface. Figures C and D represent surface and cross-sectional cuts (along δ = 90° azimuth), respectively for a S-terminated surface. Solid contours indicate an increase in electron density while dashed lines indicate electron density loss. Contours were drawn from +0.15 to -0.15 e_o/au^3 at 0.05 intervals.
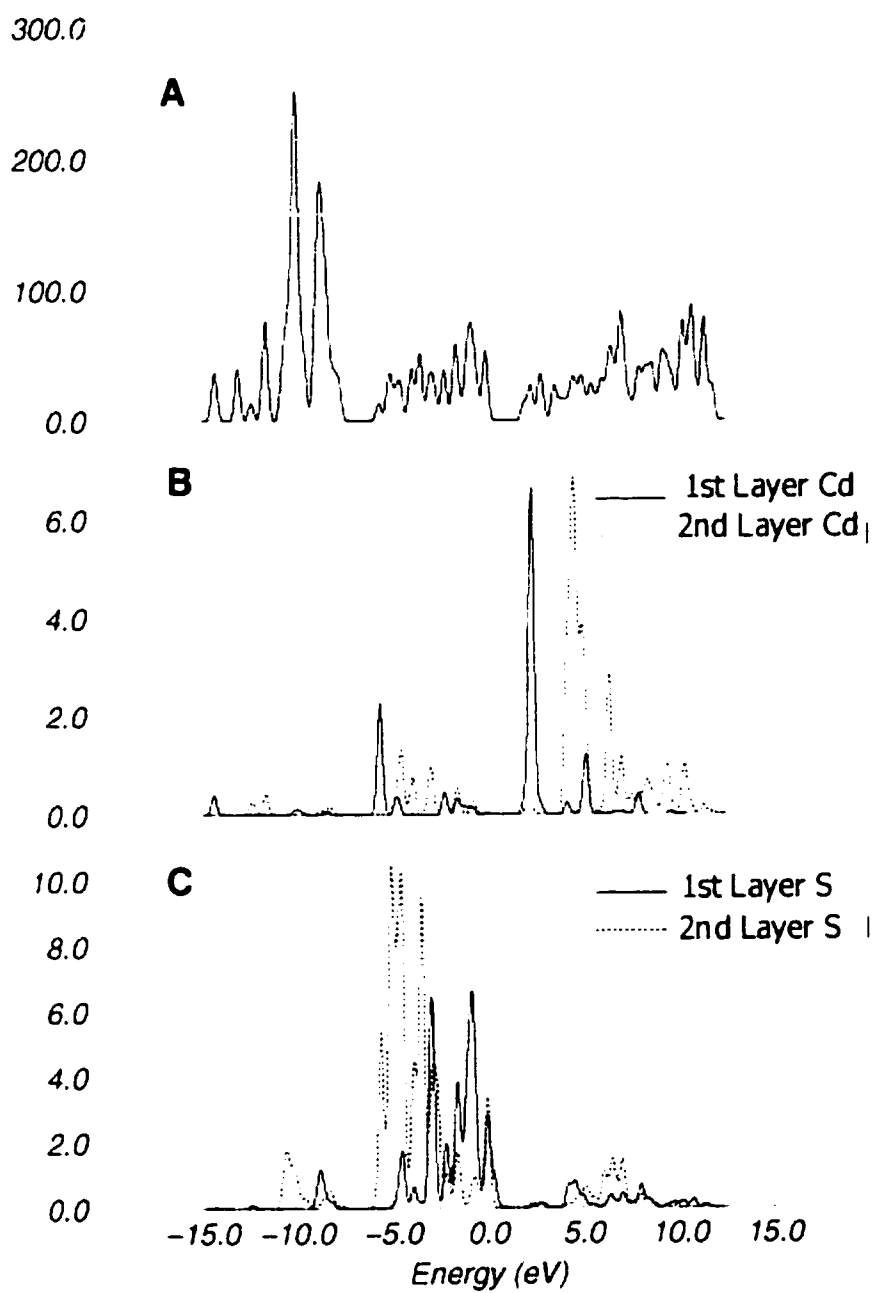
Figure 2.5 Calculated density of states for CdS cluster D of Fig. 2.3. A) Total DOS for the CdS cluster; B) PDOS for the Cd(5s) state; C) PDOS for the S(3p) state.
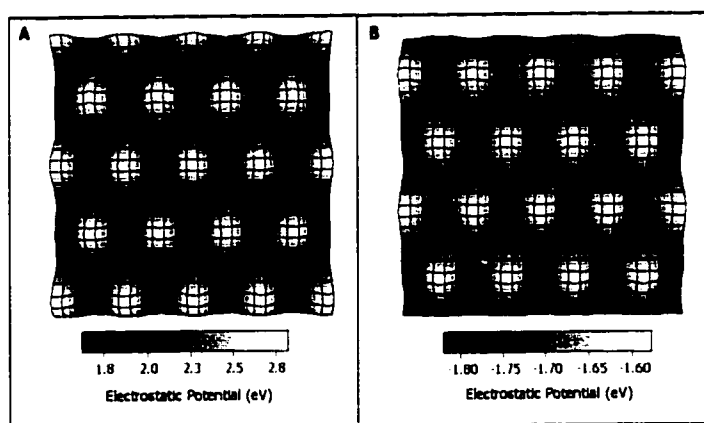
Figure 2.6 A) Lateral variation of the electrostatic potential at a distance of 4 au above the 1st-layer Cd on the Cd-terminated CdS{0001} surface; B) Lateral variation of the electrostatic potential at a distance of 4 au above the 1st-layer S on the S-terminated CdS{000$\bar{1}$} surface.
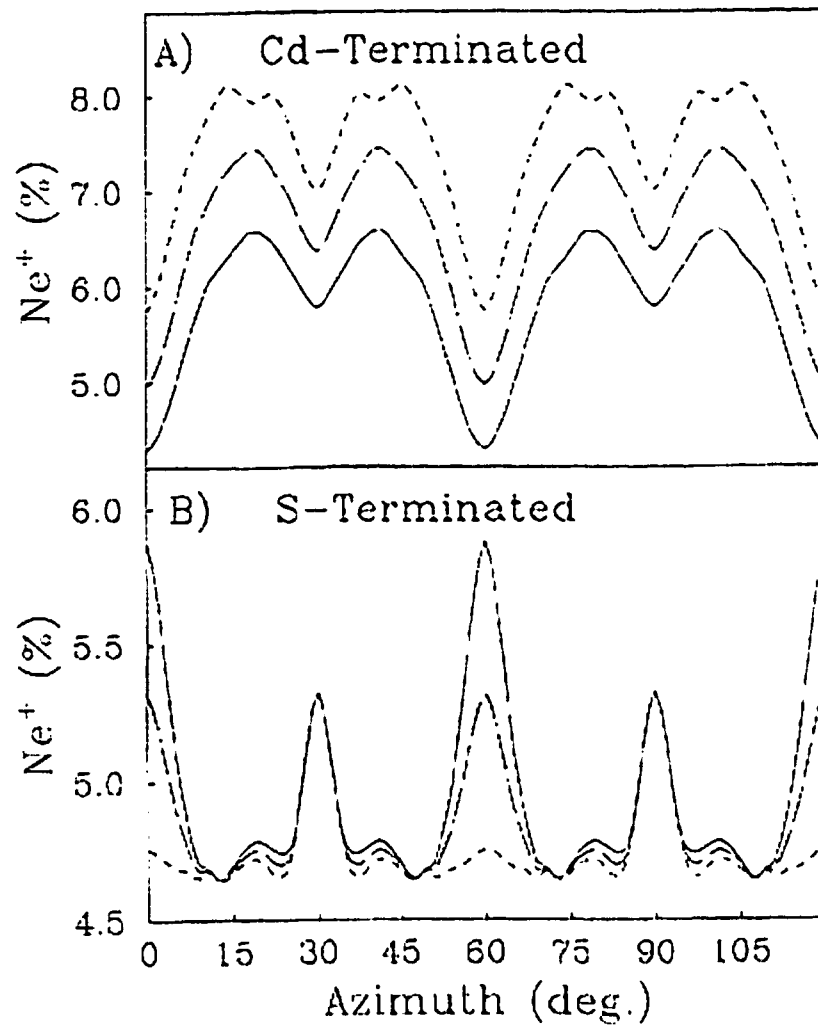
Figure 2.7 Calculated azimuthal variation of the Ne$^+$ ion fractions scattered from the CdS surfaces. A) Sensitivity of the calculated ion fractions to the radius R$_{Cd}$ on the Cd-terminated surface. The dotted, dashed and solid curves are for R$_{Cd}$ = 2.0, 2.5, and 3.0 a.u., respectively. B) Sensitivity of the calculated ion fractions to the relative weight α of the two trajectories used to model Ne scattering from the S-terminated surface. The dotted, dashed and solid curves are for α_{AB} = 0.33, 0.50, and 0.67, respectively.
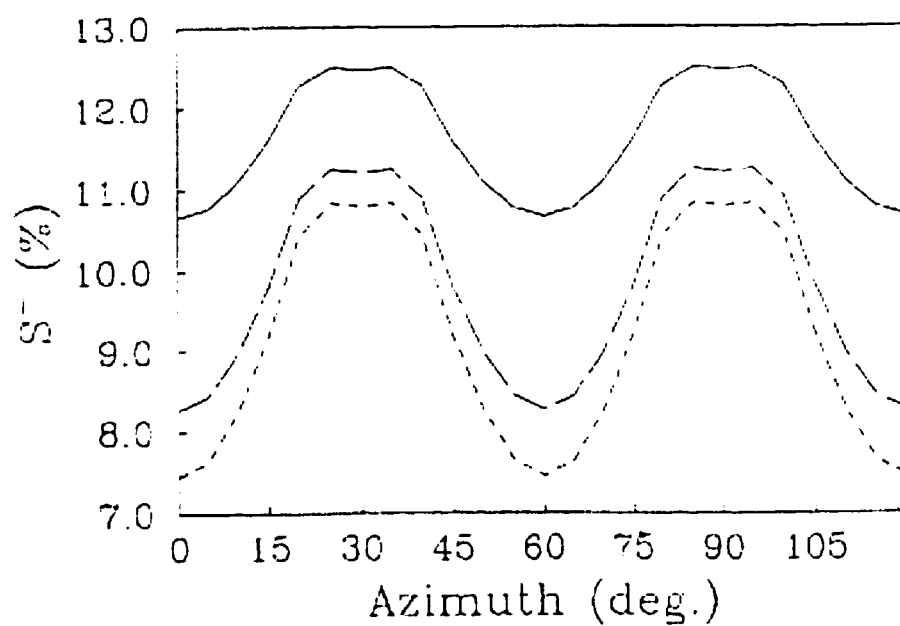
Figure 2.8 Calculated azimuthal dependence of the negative ion fraction of S⁻ recoiled from the S-terminated surface. The curves show the sensitivity of the calculated ion fractions to the parameter ξ_S^0. The dotted, dashed and solid curves are for $\xi_S^0 = 0.1$, 0.2, and 0.5, respectively.

Chapter 3

Silicon(100)-(2×1)

3.1 Intrinsic Silicon Substrate

3.1.1 Experiment

Measurement of Ne$^+$ ion scattering from the intrinsic Si(100)-(2×1) surface was carried out by Dr. Wayne Rabalais' surface physics group at the University of Houston. The measurements were carried out in a TOF-SARS spectrometer[1]. The technique uses a pulsed noble gas ion beam that is scattered from a sample surface in an ultra-high vacuum chamber. The scattered and recoiled ions plus fast neutrals are measured by TOF techniques. A 4 keV Ne$^+$ ion beam with a pulse width of ∼50 ns, pulse rate of 25 kHz, and average ion current of ∼0.1 nA/cm^2 was used. The scattered and recoiled particles were velocity analyzed through a 1.6 m long TOF drift tube and detected by a channel electron multiplier (CEM). The CEM is sensitive to both ions and fast neutrals in the keV range and its detection efficiencies for both species are similar. The ion beam incident angle was $\alpha = 9°$ with respect to the surface plane and the scattering angle was $\theta = 32°$ with respect to primary ion beam direction. Ion fractions were determined by measuring the TOF spectra with and without a voltage applied to a deflector plate near the ion flight path. The difference in the number

of particles measured with a grounded deflector plate (neutrals + ions) and with a

deflection voltage (only neutrals) gives the absolute number of ions. The ion fractions

are calculated as the ratio of the intensities as $Y = Ne^+/(Ne^o + Ne^+)$. The sample

was a Si(100) p-type wafer with a conductivity of 10 - 20 Ω-cm. The scattered Ne^+

ion fractions Y are highly sensitive to the alignment of the ion beam with the crystal

azimuthal directions, δ. Plots of scattering intensity I(δ) versus the crystal azimuthal

angle δ were made by maintaining the ion beam at a fixed incident angle and rotating

the crystal about the surface normal. TOF spectra were acquired at $\delta = 2°$ intervals.

Azimuthal scans of the scattered Ne^+ ion fractions, Y, are shown in Fig. 3.1. Both

the scattered Ne intensities and the ion fractions exhibit periodic behavior with a 45°

cycle. This reveals that the Si(100) surface consists of two domains that are rotated

by 90° with respect to each other. Si(100) is known to undergo a (2×1) reconstruction

in which pairs of surface atoms move close together to form dimers in the first layer.

Models of the surface are shown in Fig. 3.1. illustrating the atomic alignments of the

dimers for the case of two single (2×1) domains rotated by 90° from each other. If

the two (2×1) domains are present with equal probability, the macroscopic ion beam

samples a surface whose total symmetry is similar to that of the overlapped domains.

The scattering and recoiling imaging code (SARIC)[2] was used to simulate the

scattering intensity as a function of δ. The results are shown in Fig. 3.2 for the

Si(100)-(2×1) two-domain surface with the same conditions used in the experiments,

i.e. $\alpha = 9°$ and $\theta = 32°$. The effect of two domains, orthogonal to each other, was incorporated into the simulation by constructing a surface such as that shown in Fig. 3.3. with two domains of equal probability rotated by 90° with respect to each other. The positions of the simulated intensity maxima and the repetition of the symmetry features every 45° are consistent with the experimental intensity results of Fig. 3.1.

The depth of penetration of the trajectories is extremely sensitive to the azimuthal direction of the impinging atoms. The percentage of the Ne atoms that collide with the 1st-. 2nd-, and 3rd-layers of the two-domain $Si(100)$-(2×1) surface as a function of azimuthal angle are plotted in Fig. 3.2. The highest percentage of scattered Ne atoms originates from the 1st-layer. followed by 2nd-layer scattering and then 3rd-layer scattering. The probabilities of scattering from these various layers is strongly dependent on the azimuthal direction of the impinging Ne^+. The scattering intensity from the 1st-layer is minimum along the high symmetry directions of $0°$. $45°$. and $90°$ where penetration occurs, whereas the scattering intensity from the 2nd- and 3rd-layers is maximum along these high symmetry directions.

3.1.2 Theoretical Approach

It is the goal of this work to draw a correlation between the Ne^+ neutralization rates and the local charge density encountered by the ion along its scattering trajectory. Many current charge transfer models depend, ultimately, upon a dynamic charge

density description of the donor and acceptor sites. It is tempting to investigate if such a correlation applies in an ion-surface neutralization event. The electronic structure of the Si(100)-(2×1) surface was calculated using ab initio electronic structure methods employing the density functional approximation[14].

Calculations were performed on a cluster consisting of 117 atoms, modeling the topmost four layers of the experimental Si target surface. The charge density in the interior part of this cluster was found to be well converged. The charge density of the infinite surface was generated by translation of the charge density from a unit cell in the interior part of the cluster. The electronic charge density $\rho(\vec{R})$ of the reconstructed Si surface is shown in Fig. 3.3. The figure shows the accumulation of charge density near the Si dimers. Since the charge distribution, as a result of the dimerization, presents local azimuthal anisotropy, we can expect this azimuthal variation to be reflected in the charge transfer rates for the incident Ne^+ ions. Mulliken charge analysis of the model Si(100) surface shows that the dimerized Si atoms on the reconstructed surface carry a charge of 0.055 e_o. Similar calculations for an unreconstructed Si(100) surface have a charge of 0.113 e_o. This charge rearrangement indicates the stabilization of the reconstructed (2×1) surface, the surface atoms of the reconstructed system approaching the charge state of the bulk molecular silicon atoms. The neutralization rate of Ne^+ impinging on a surface can be obtained by integrating the following rate equation along the trajectory of the ion.

$$\frac{dI}{dt} = -\Gamma(\vec{R}(t))I(t) \tag{3.1}$$

In this equation, $I(t)$ is the instantaneous ion fraction and is the neutralization probability at $\vec{R}$. We now make the simple assumption that the neutralization probability at position $\vec{R}$ is proportional to the local substrate charge density $\Gamma(\vec{R}(t)) = \alpha\rho(\vec{R})$. For a kinetic energy of 4 keV, the separation between the Ne and Si atoms at the closest encounter is 0.6 a.u. In this region the substrate charge density is dominated by the electron density for the core states of the Si atom. These electrons will not participate in the neutralization of the Ne(2p) hole due to their extremely large binding energies. We do not expect neutralization of Ne$^+$ to take place at such close proximity to the Si atoms, and therefore introduce a cut-off radius, $\vec{R}_c$, around each Si atom within which the neutralization rate Γ is assumed to be zero. Neutralization of Ne$^+$ arises mainly from the more loosely bound valence electrons.

Using the calculated charge density , Eq. 3.1 can be integrated along the trajectories of the Ne$^+$ ions. The resulting ion-fraction takes the form

$$I(\delta) = exp[-\frac{\alpha}{v} \int_{-\infty}^{\infty} dR\rho(R,\delta)] \tag{3.2}$$

where it is assumed that the ion moves with a constant velocity, v. The quantity in the exponent is proportional to the integrated charge density along the path of the ion. The pronounced charge asymmetry caused by the reconstruction of the surface

atoms introduces an azimuthal dependence of the ion fractions. The reconstruction of the surface also increases the possibility for subsurface, i.e. 2nd-, 3rd-, and 4th-layer, Ne-Si collisions. The ions that undergo subsurface trajectories will encounter regions of much larger valence electron densities than the atoms scattering from the surface atoms and will therefore be neutralized with high probability. For this reason, it is not important to know the details of the subsurface trajectories. However, the fraction of ion trajectories that take subsurface paths needs to be determined. The trajectory simulations performed using the SARIC algorithm (Fig. 3.2) indicate that the fraction of subsurface trajectories $\beta(\delta)$ at $\alpha = 9°$ is large and strongly dependent on azimuthal angle δ. The azimuthal dependence is caused by the anisotropy of the reconstructed surface. The resulting final ion fractions for Ne^+ scattered from the Si(100)-(2×1) surface can be described by accounting for both the surface and subsurface collisions

$$I(\delta) = I_{subsurf}(\delta)\beta(\delta) + I_{surf}(\delta)[1 - \beta(\delta)] \qquad (3.3)$$

where the subsurface ion fraction, $I_{subsurf}(\delta)$, does not contribute, as all ions undergoing subsurface collisions are assumed to be neutralized. The final ion fraction can then be expressed as

$$I(\delta) = [1 - \beta(\delta)]exp[-\frac{\alpha}{v} \int_{-\infty}^{\infty} dR\rho(R,\delta)] \qquad (3.4)$$

3.1.3 Results

Trajectory integrated charge densities were calculated for each atom of the target dimer independently and the results were averaged for identical azimuths. The experimental ionization fractions were taken from a reconstructed Si surface consisting of two domains rotated 90° relative to each other. In order to model the two surface domains in this system, the path-integrated charge densities were rotated 90° and averaged.

The parameter α was obtained by fitting the experimental data. In the present work, α/v was found to be 1.4 au^2/e_o, giving $= 3.7 \times 10^{15}$ au^3/e_o-sec. In the limit $\alpha/v \to 0$, the final ion fraction simply becomes the fraction of surface collisions. The final calculated ion fraction is shown as a function of azimuthal angle δ in Fig. 3.4. The figure also shows the azimuthal variation of $(1-\beta(\delta))$. It can clearly be seen that the calculated azimuthal dependence of the surviving ion fractions is in qualitative agreement with the experimental data. The largest ion fractions are observed at $\delta = 20°$, 70° and the minimum ion fractions occur at $\delta = 0°$ and 45°. It can also be seen that $(1 - \beta(\delta))$ correlates well with the experimental data. It is this factor in Eq. 3.4 that leads to the pronounced azimuthal dependence of the measured ion fractions. The reason for this is that the subsurface charge density is an order of magnitude greater than the surface charge density. The subsurface collisions therefore result in a very high probability of Ne^+ neutralization. The variation of the surface electronic

charge density and its influence on charge transfer contributes little to the overall variation of the final neutral fractions recorded in this experiment - the dominant factor being the relative difference in magnitude of the surface/subsurface charge densities of the target surface.

A detailed comparison of the theoretical results in Fig. 3.4 and the experimental data in Fig. 3.1 reveal some discrepancies. In particular it can be seen that the calculated ion fraction maxima are considerably broader than the corresponding peaks in the experimental data. Such a discrepancy may be due to our simple parameterization of the local charge transfer probability, our neglect of substrate atom recoil, the use of an approximate ion-surface interaction potential, and/or the assumption of linear trajectories of the ions. A more extensive investigation including the integration of charge transfer probabilities along realistic trajectories of the atom must be undertaken before any definite conclusion of the validity of the model can be drawn.

3.2 n- and p- doped Silicon Substrates

3.2.1 Experiment

Measurement of experimental ion fractions for Ne^+ ion scattering from n-, p-doped and intrinsic Si(100)-(2×1) surfaces was once again accomplished by Dr. Wayne Rabalais' group at the University of Houston. The measurements were made in a TOF-SARS spectrometer [1] using a 4 keV Ne^+ beam (pulse width of ∼50 ns, pulse

rate of 25 kHz, and ion current $\sim$ 0.1 nA/cm^2). The scattered and recoiled ions

plus fast neutrals were measured by TOF techniques using a 1.6 m long TOF drift

tube and detected by a channel electron multiplier. The ion beam incident angle

was α = 12° with respect to the surface plane and the scattering angle was θ = 32°

with respect to primary ion beam direction. Scattered on fractions, Y = Ne$^+$/(Ne^o

+ Ne$^+$), were determined by measuring TOF spectra with and without a voltage

applied to a deflector plate near the ion flight path. The difference in the number of

particles measured with a grounded deflector plate (Ne^o + Ne$^+$) and with a deflection

voltage (Ne^o) gives the absolute number of ions. The samples were heavily doped

n- and p-type Si(100) wafers with resistivities of 0.005-0.020 and 0.004-0.025 Ω-cm,

respectively. The cleaning procedure consisted of sequences of Ar+ bombardment (2

$\times$ 10^{-5} Torr Ar, 0.5 keV, 1 μA) followed by annealing at 900°C with gradual cooling.

This treatment produced a sharp (2×1) LEED pattern with no impurities detectable

by TOF-SARS.

Plots of scattering intensity I(δ) versus the crystal azimuthal angle δ were made by

maintaining the ion beam at a fixed incident angle α and rotating the crystal about

the surface normal. TOF spectra were acquired at δ = 2° intervals. The azimuthal

scans of the scattered Ne ion fractions Y determined from these scans are shown in

Fig. 3.1. A periodic behavior with a 45° cycle is observed. Si(100) undergoes a (2×1)

reconstruction in which dimers are formed in the first layer. The two (2×1) domains

are rotated by 90° with respect to each other and are present with equal probability. The macroscopic ion beam samples a surface whose total symmetry is similar to that of the overlapped domains, hence the 45° periodicity.

3.2.2 Theoretical Approach

The final ion fraction of Ne^+ scattered from Si(100) 2×1 reconstructed surfaces indicates that ion neutralization rates depend significantly upon target doping densities. Scattering from antimony doped, n-type silicon surfaces presents almost no change in the final ion fraction when compared to the same experiment performed on structurally identical, intrinsic Si. However, final ion fractions for Ne^+ scattering from structurally identical boron doped, p-type silicon surfaces indicates a strong decrease in the ion neutralization rate when compared to the intrinsic Si target. Since the surface geometry for all three samples is identical (n-type, p-type and intrinsic) any variation in neutralization rate must come from a difference in electronic structure.

The effects of local charge density upon Ne^+ atom neutralization during collisions with the Si(100)-(2×1) surface can be described using the simple rate equation approach outlined earlier (Eqs. 3.1-3.4). Since it is not possible to reflect semiconductor doping in finite cluster models on the order of $\sim$100 atoms, analytical band structure arguments must be applied to describe the observed differences between the intrinsic, n- and p-type surfaces.

3.2.3 Results

The charge density of the Si(100) 2×1 surface (intrinsic) was calculated using a density functional electronic structure algorithm [16]. A finite cluster model of 117 atoms was used to calculate the charge density in a unit cell of the Si surface. This unit cell was then repeated to reproduce a Si surface of arbitrary size. The charge density distribution was used in Eq. (3.4) to determine the theoretical final ion fraction as a function of azimuthal incidence angle, δ. The parameter α in Eq. (3.4) was obtained by fitting the calculated ion fractions to experimental data. The best fit values for α/v were 1.955 and 1.365 for the n-type and p-type scattered ion fractions, respectively.

Figure 3.5 indicates reasonable agreement between the experimental data and the theoretical fit. As discussed in ref. [17], the ion fractions from all of the Si substrates reflect the local charge density encountered by the scattered ion. Trajectories that pass through several surface dimers (azimuth, $\delta = 0, 90$), encounter a high charge density compared to other azimuths. This results in a higher neutralization probability, lowering the ion fraction (as expressed in Eq. (3.4)). The fitted parameter α/v indicates a low neutralization probability for Ne^+ scattered against the p-type Si surface when compared to the neutralization probability when scattered against intrinsic and n-type surfaces. Qualitatively, this result may be explained by examination of the electrostatic potential caused by the surface band bending on the different n-, p-doped, and intrinsic surfaces.

The relative strength of surface band bending can be determined from the doping density of the substrates, measured as a function of substrate resistivity. Resistivity measurements for the doped silicon substrates yield values of 0.004-0.025 Ω-cm and 0.005-0.020 Ω-cm for the p- and n-type surfaces, respectively. Calculation of doping density based on these resistances gives a range of $2.5 \times 10^{18} - 2.5 \times 10^{19}$ cm^{-3} for the p-type Si and a range of $1.0 \times 10^{18} - 1.1 \times 10^{19}$ cm^{-3} for the n-type Si, indicative of highly doped substrates. At room temperature complete ionization of both donor and acceptor states can be assumed, placing the Fermi energy, E_f, near the valence band for the p-type Si and near conduction band for the n-type Si. Fermi surface pinning at the surface has been measured as $E_f - E_{vs} = 0.32 \pm 0.02$[18]. This results in an upward band bending of 0.88 eV for n-type Si and 0.26 eV for the intrinsic Si while p-type Si experiences a downward band bending of 0.31 eV at the surface.

The downward band bending observed in the intrinsic and n-doped Si creates a depletion layer of majority carriers (electrons) near the surface and a complimentary population of surface states to maintain surface neutrality [19]. The depletion layer produces a positive space charge due to the presence of positively charged donor atoms at the surface [20, 10]. Both of these effects may facilitate charge transfer at the surface. Population of surface states necessarily increases the charge density at the substrate surface, increasing the total integrated charge density along the ion trajectory (Eq. (3.2)). A positive space charge presents an attractive potential to

the Ne(2p) level, lowering the charge barrier and enhancing charge transfer from the surface to the ion[21]. The upward band bending observed in the p-doped Si creates a depletion layer of majority carriers (holes) resulting in a negative space charge near the surface and leaves surface states unpopulated[10, 20]. A negative space charge produces a repulsive potential, increasing the tunneling barrier and reducing the neutralization probability[21]. The accumulation of charge at the p-doped interface is the result of negatively charged acceptor atoms. Such localized charge should play a significantly smaller role in charge transfer compared to the more energetic, occupied electron surface states found on the intrinsic and n-doped substrates.
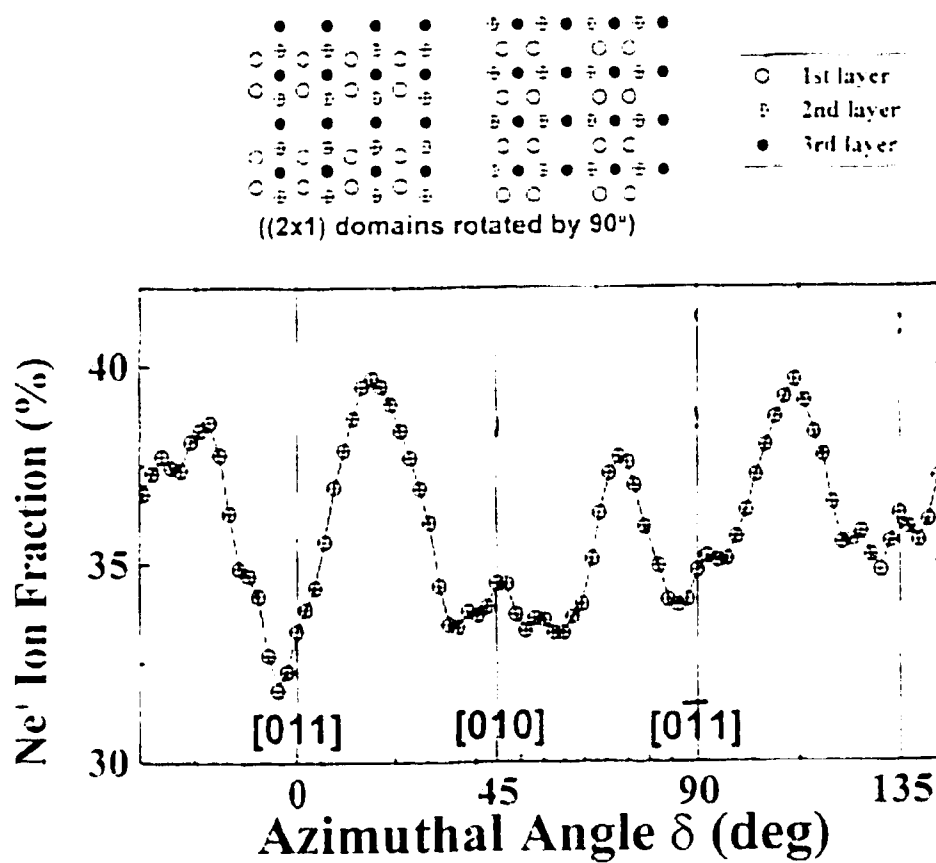
Figure 3.1 Experimental scattered Ne$^+$ ion fractions from intrinsic Si(100)-(2×1) surface. The figures above the graph represent single (2×1) domains rotated by 90°.
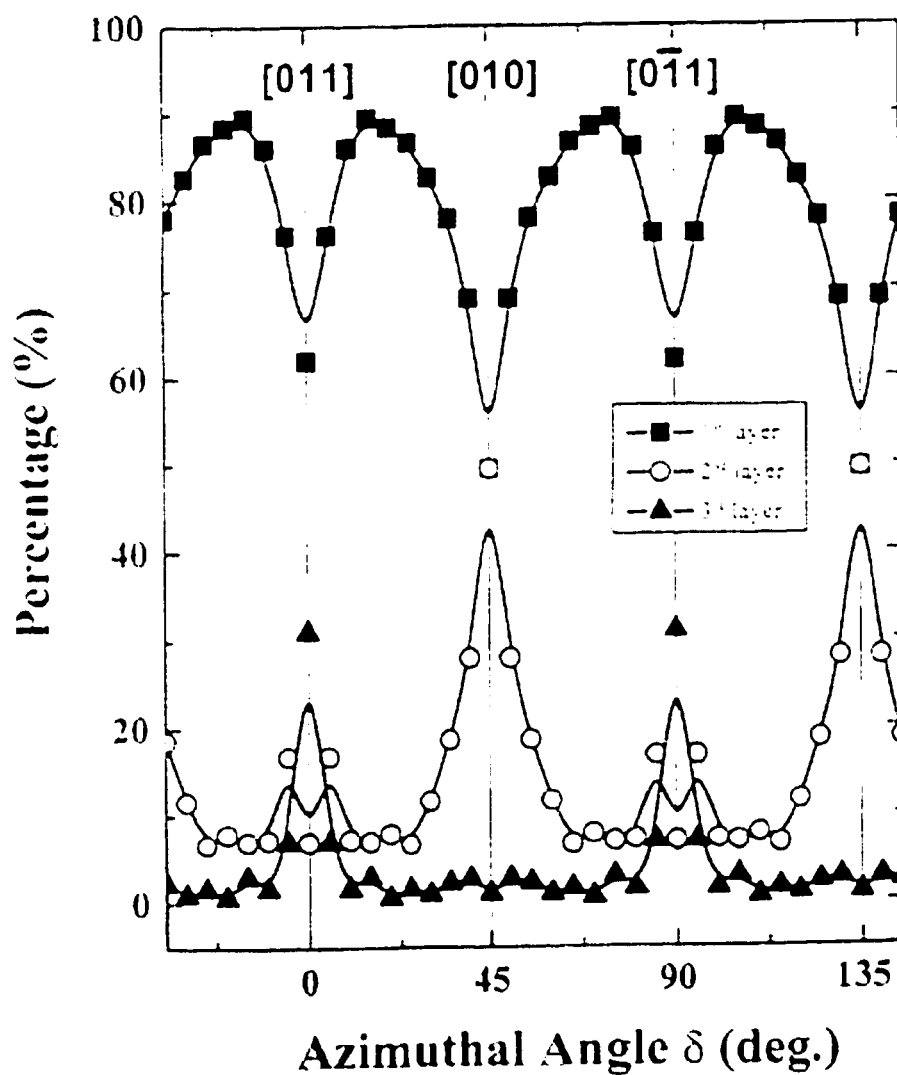
Figure 3.2 Percentage of Ne^+ ion trajectories that scatter from the 1st, 2nd and 3rd layers of the Si(100)-(2×1) two-domain surface as a function of azimuthal angle δ from SARIC simulations.
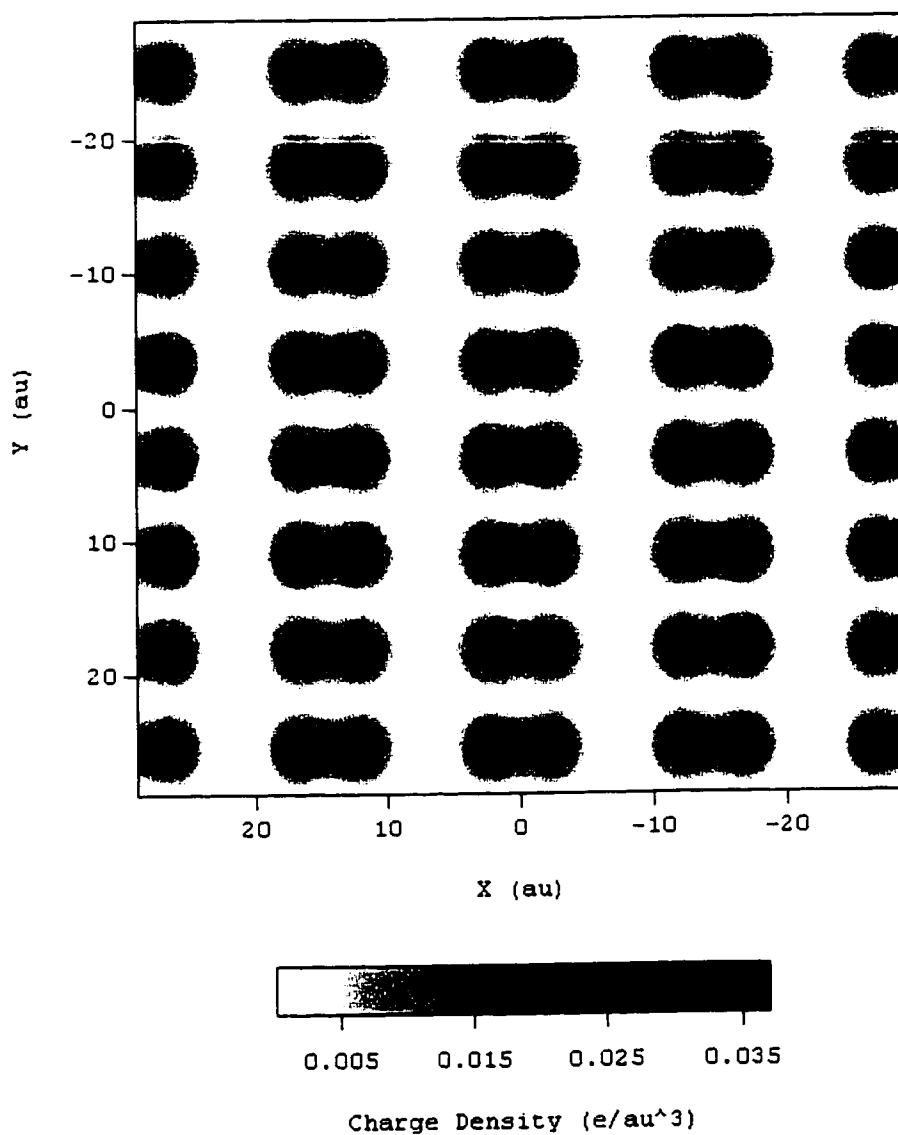
Figure 3.3   Calculated surface electronic charge density of Si(100)-(2×1) at 5 a.u. above the first Si layer.
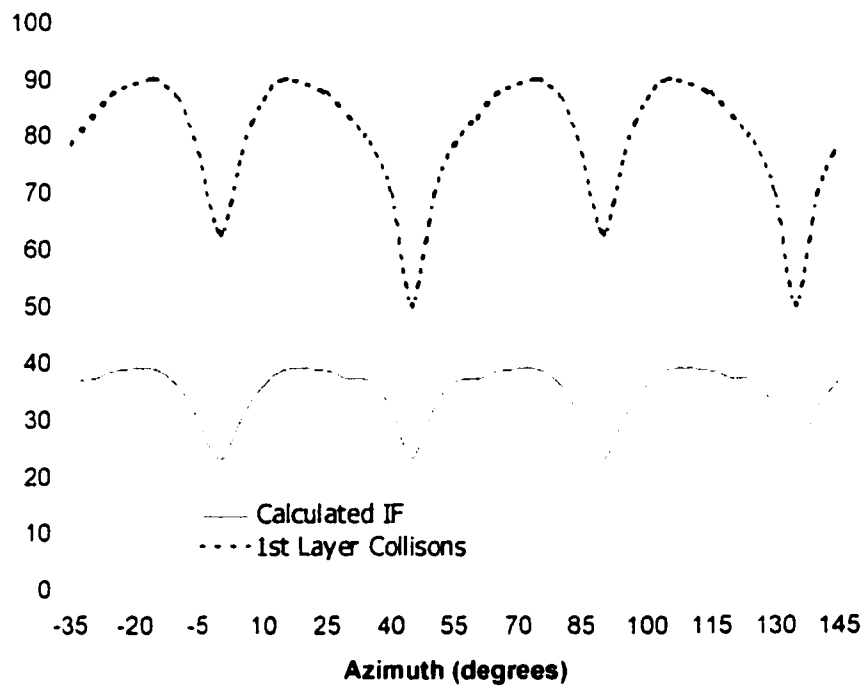
Figure 3.4 Calculated azimuthal variation of Ne$^+$ ion fractions (domain averaged) and the fraction of ions scattered from the topmost surface layer $(1-\beta(\delta))$.
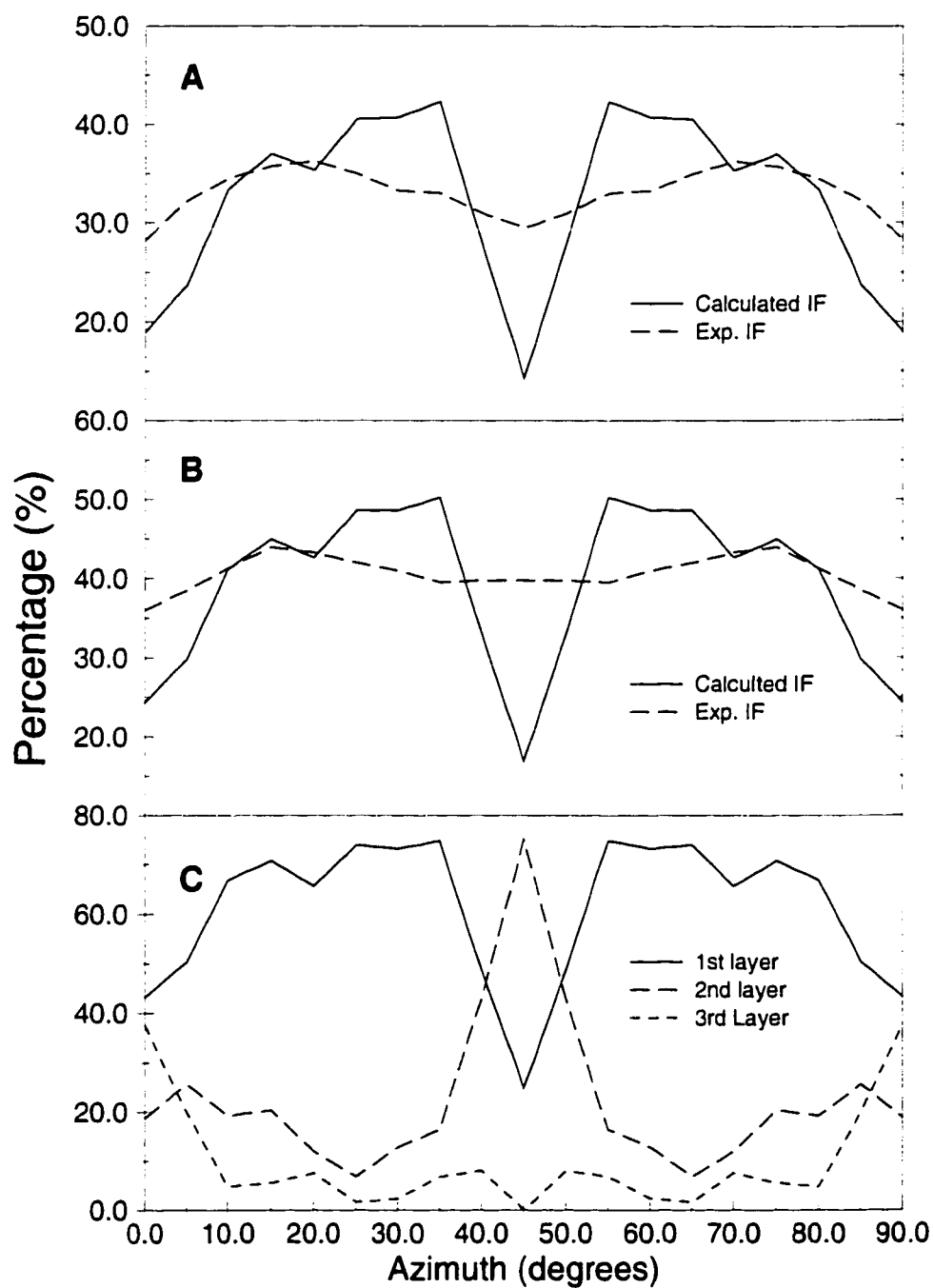
Figure 3.5 Comparison of experimental and calculated ion fractions for doped Si substrates. A) Ion fractions for n-doped Si target surface; B) Ion fractions for p-doped Si target surface; C) Percentage of ions scattered from the 1st, 2nd and 3rd layers of the Si(100)-(2×1) surface.
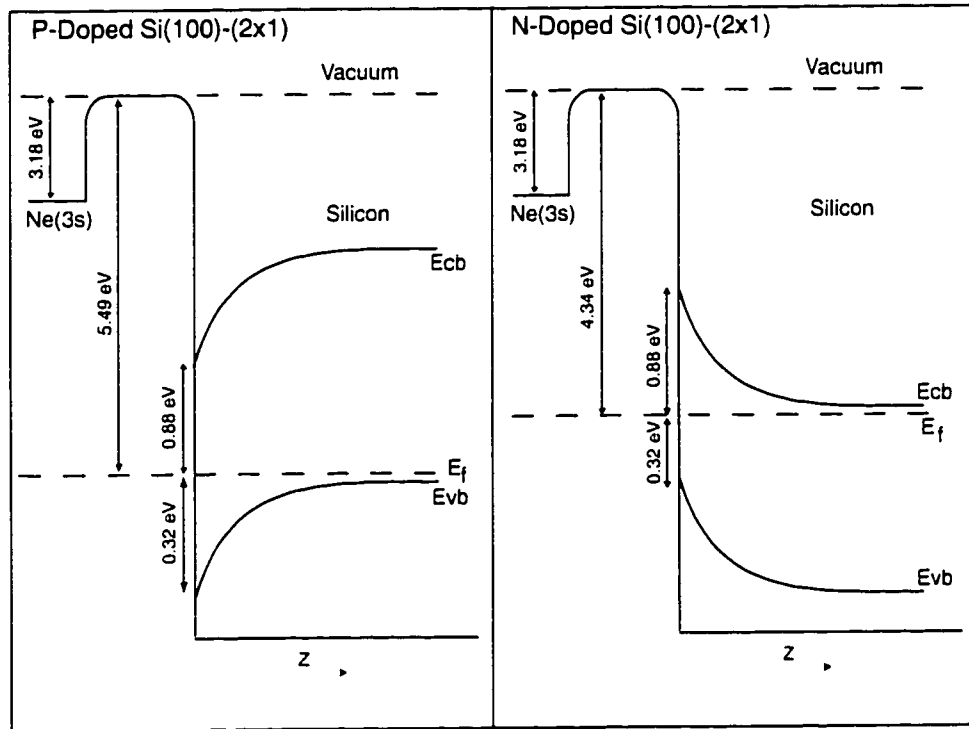
Figure 3.6 Illustration of band bending at the Si surface for n-doped and p-doped substrates. E_f, E_{vb}, and E_{cb} indicate the positions of the Si Fermi level, the Si bulk valence band and the Si bulk conduction band, respectively. The Z axis starts at the Si surface and moves towards the bulk (to the right).

Chapter 4

Conclusion

4.1 CdS

The magnitudes and azimuthal anisotropies of Ne^+ scattered ion fractions from both the Cd- and S-terminated surfaces of CdS{0001} are highly sensitive to both surface structure and electron density. There is a clear correlation between the experimentally observed ion fractions and the lateral variation of the electrostatic potential on the surfaces. This correlation is believed to be caused by the variations in surface to atom electron transfer rates due to tunneling barriers introduced by the electrostatic potential on the surfaces. The calculations have provided a microscopic understanding of the experimental data. The essential physics is a lateral variation of electron tunneling rates between an atom and the surface caused by a nonuniform electrostatic potential. The accumulation of electrons near the surface S atoms introduces a repulsive potential energy for a tunneling electron. This reduces electron tunneling rates near surface S atoms. For Cd, the situation is opposite. The depletion of electronic charge near surface Cd atoms increases the tunneling rates near these atoms. The parameters used in the proposed model all have reasonable magnitudes [22, 23, 24]. However, due to the simplicity of the model, these parameters may not have quanti-

tative significance outside of the present context. The major deficiency of the present model is the use of idealized trajectories to describe the motion of the ions. The finding of a strong trajectory dependence of the charge transfer probability suggests that the rate equation (Eq. 2.1) should be integrated along realistic trajectories. This represents a major undertaking but will be attempted in the near future.

4.2 Si(100)-(2×1)

The experimental results in Fig. (3.1) can be qualitatively explained with the above arguments. Collisions between Ne^+ and a p-doped Si substrate yield lower charge neutralization rates when compared to intrinsic and n-type Si surfaces due to the presence of a repulsive surface potential and the low occupation of surface states. The comparatively low ion fractions observed in Ne^+ collisions on n-type and intrinsic Si surfaces are reflective of an increased charge density due to the occupation of surface states and a reduction of the charge tunneling barrier arising from the positive surface space charge. The similarity between the intrinsic and n-doped Si surface electrostatic potential arising from the downward band banding observed for both materials is responsible for the identical ion fractions observed for these two substrates. Both surfaces experience an upward band bending, resulting in occupation of surface states and a positive surface space charge. When compared to the overall surface charge, the relative change between the n-doped and intrinsic substrates is negligible, and

should not contribute to the overall neutralization probability for incident Ne^+ ions.

A change in the ion fraction is observed only for a repulsive tunneling barrier and a loss of charge density from the unoccupied surface states, as found in a p-doped substrate.

Bibliography

[1] O. Grizzi, M. Shi, H. Bu, and J. Rabalais, Rev. Sci. Instrum. **61**, 740 (1990).

[2] V. Bykov *et al.*, Nucl. Instrum. Methods Phys. Res. Sect B **114**, 371 (1996).

[3] U. von Barth and L. Hedin, J. Phys. C **5**, 1629 (1972).

[4] L. Lou, T. Guo, P. Nordlander, and R. E. Smalley, J. Chem. Phys. **99**, 5301 (1993).

[5] K. Chang, S. Froyen, and M. L. Cohen, Phys. Rev. B **28**, 4736 (1983).

[6] J.Ahn and J. W. Rabalais, J. Phys. Chem. B **102**, 223 (1998).

[7] P. Nordlander and N. Lang, Phys. Rev. **B44**, 13681 (1991).

[8] M. Cardona, M. Weinstein, and G. A. Wolff, Phys. Rev. **140**, A633 (1965).

[9] C. Kittel, *Introduction to Solid State Physics* (Wiley, New York, 1996).

[10] A. Zangwill, *Physics at Surfaces* (Cambridge, Cambridge, 1988).

[11] J. F. Zeigler and U. L. J. P. Biersack, *The Stopping Power of Ions in Solids* (Pergamon, New York, 1985).

[12] J. W. Rabalais, CRC Crit. Rev. Sol. St. & Mat. Sci. **14**, 319 (1988).

[13] D. C. Langreth and P. Nordlander, Phys. Rev. **B43**, 2541 (1991).

[14] J. Mackey, L. Lou, and P. Nordlander, J. Chem. Phys. **102**, 7484 (1995).

[15] A. G. Borisov, G. E. Makhmetov, D. Teillet-Billy, and J. P. Gauyacq, Surface Sci. **350**, L205 (1996).

[16] L. Lou, P. Nordlander, and B. Hellsing, Surf. Sci. **320**, 320 (1994).

[17] I. Vaquilla *et al.*, J. Chem. Phys. **To Be Published**, (2000).

[18] W. Monch, P. Koke, and S. Krueger, J. Vacuum Sci. Technol. **19**, 313 (1981).

[19] J. Bardeen, Phys. Rev. **71**, 717 (1947).

[20] W. Monch, *Semiconductor Surfaces and Interfaces* (Springer, Berlin, 1995).

[21] L. Houssiau, J. W. Rabalais, J. Wolfgang, and P. Nordlander, Phys. Rev. Lett. **23**, 5153 (1998).

[22] J. P. Gauyacq and A. G. Borisov, Condens. Matter **10**, 6585 (1998).

[23] P. Nordlander and J. C. Tully, Phys. Rev. **B42**, 5564 (1990).

[24] C. C. Hsu, A. Bousetta, J. W. Rabalais, and P. Nordlander, Phys. Rev. **B47**, 2369 (1993).